Sorption Enhanced Steam Reforming SESR of acetic acid and model compounds complex mixture with Ni-based catalysts on alumina and olivine

E. Acha*[1], D. Chen[2], J.F. Cambra[1]

[(1)] *Chemical Engineering and Environmental Department, Engineering Faculty of Bilbao, University of the Basque Country (UPV/EHU), Alameda Urquijo s/n, 48013 – Bilbao (Spain)*

[(2)] *Department of Chemical Engineering, Norwegian University of Science and Technology, Sem Sælands vei 4, Trondheim 7491, Norway*

[(*)] corresponding author: esther.acha@ehu.es

Keywords: Hydrogen, bio-oil, reforming, SESR

Abstract

Seven Ni-based catalysts were prepared over different supports (conventional Al_2O_3, non-conventional olivine and hydrotalcite) with Co and Pd addition. Their catalytic performance was studied in hydrogen production by stean reforming (SR) and sorption enhanced steam reforming (SESR) of acetic acid as model compound and a mixture of acetic acid, acetone, phenol, furfural and 1-butanol as a simulated bio-oil. Two dolomites were employed as CO_2 sorbents and compared. The so-called Norway dolomite showed better characteristics for CO_2 sorption than Castro dolomite. High purity hydrogen (99%) was generated during the SESR process without CO or CH_4 detection, before the breakthrough curve, even during the complex mixture reforming. The non-conventional support catalysts showed very good performance with high hydrogen purity, hydrogen yields and good stability during 20-50 h under reforming conditions.

1 Introduction

Hydrogen is one of the candidates to replace the current main transport energy vectors and it can also be used for power and heat generation on demand. Hydrogen fuel cells are environmentally friendly, as they are able to convert directly chemical energy into electricity. However, nowadays there are some difficulties for hydrogen economy implantation, and one of them is the high purity required for hydrogen. This energy vector is still being mainly produced from fossil fuels, from which hydrogen is produced as a component of a mixture containing other gases such as CO, CO_2, H_2O and unreacted gases. In reforming reactions the main by-product gas is carbon dioxide.

There are three basic methods to separate CO_2 from the mixture: separation with sorbents/solvents, separation with membranes, and separation by cryogenic distillation. Among these strategies, the sorption enhanced steam reforming (SESR) process is attracting a great deal of attention because it combines both hydrogen production and CO_2 separation. In the SESR process, carbon dioxide is captured by an in situ sorbent, which shifts the reversible reforming and water gas shift (WGS) reactions to the product side beyond their conventional thermodynamic limits, giving rise to a higher hydrogen production [1] and lower cost [2].

The potential benefits of producing H_2 by SESR concept are:

1. Reforming at a significantly lower temperature (400-500 ºC) than a conventional SR process, while achieving high conversion to hydrogen.
2. Production of hydrogen at feed gas pressure and at relatively high purity directly from the reactor.
3. Significant reduction or even elimination of downstream hydrogen purification steps.
4. Reduction of CO in the SESR reactor effluent to ppm levels – elimination of shift reactors.
5. Minimization of side reactions, e.g., coking.
6. Reduction of the excess steam used in conventional SR.

Complete environmental benefits of introducing hydrogen in the current energy, heat and transport economy will only be possible if this hydrogen is produced from renewable sources. There are different ways of producing "green hydrogen" such as from solar and wind produced electricity surplus or from biomass. In the case of solar and wind, hydrogen has to be produced decentralized, where the installations are located; whereas in the case of biomass bigger, more centralized and more efficient installations may be built. The employ of biomass for hydrogen production is a greener route than the actual one, since its net contribution to the increase of atmospheric CO_2 is much lower than employing fossil fuels.

Different routes for hydrogen production from biomass can be employed. Flash pyrolysis is presented as an attractive method to produce bio-oils from different types of biomass, which can later be catalytically reformed to generate hydrogen. Bio-oils are complex mixtures and very variable, depending on the raw material being pyrolized and on the conditions of the pyrolysis [3]. Acetic acid is the most representative constituent of the water soluble fraction of bio-oils, but also other compounds such as aldehydes, alcohols, carboxylic acid, cresols and ketones among others are produced [4,5]. Acetic acid is being widely employed as model compound for hydrogen production from catalytic conventional reforming of bio-oils [6–10]. There are also some works where other model compound or a more complex mixture is reformed [11–14], and even some ones where directly bio-oil is employed [15–17]. As a reference, the overall reforming reaction of acetic acid is shown in Eq. (1), which is a combination of reforming and water gas shift, Eq. (2):

$$CH_3COOH\ (g) + 2H_2O\ (g) \leftrightarrow 4H_2\ (g) + 2CO_2\ (g) \qquad \Delta H^o = +\ 184\ kJ/mol \qquad (1)$$

$$CO\ (g) + H_2O\ (g) \leftrightarrow H_2\ (g) + CO_2\ (g) \qquad \Delta H^o = -\ 41\ kJ/mol \qquad (2)$$

The reforming reactions are highly endothermic, while the water gas shift reaction is moderately exothermic. This process is thermodynamically limited and it is not possible to achieve complete conversion of reactants. In the SESR process the CO_2 is directly removed from the reaction, employing an appropriate solid sorbent, which shifts the reaction allowing a higher conversion and higher purity of produced hydrogen.

Depending on the employed sorbent, this may react with the CO_2 to generate a carbonate or the CO_2 may be physically or chemically adsorbed on its surface. The most widely employed sorbents in the literature are the calcium-based ones [18]. Xie et al. [19] performed thermodynamic analysis with nine CO_2 sorbents in the co-existence of CO_2 and H_2O and they also concluded that CaO had the best capacity in the temperature range (325-727 ºC). A nice sorbents' review is done already in the work by Dou et al. [20].

The carbon dioxide capture of a CaO-based sorbent is:

$$CO_2\ (g) + CaO\ (s) \leftrightarrow CaCO_3\ (s) \qquad \Delta H^o = -\ 178\ kJ/mol \qquad (3)$$

In the carbonation process of CaO there is an initial fast step controlled by chemical kinetics, and a second and slower step controlled by the diffusion in the created product ($CaCO_3$) [21]. This reaction is exothermic and it is thermodynamically favoured at lower temperatures and higher pressures. The SESR process with CaO-based sorbent could be almost thermally neutral, but energy is required for its regeneration. In spite of considering the energy employed for the regeneration, the supplemental energy required for the whole conventional steam reforming process is still less [20].

The CaO-based sorbents present two main advantages: their raw materials are inexpensive and abundant (i.e. limestone or dolomite) and they exhibit good kinetics and sorption capacities at high temperatures (400-650 ºC) [22]. Limestone has the advantage of wider availability and a higher theoretical capacity of 0.79 g_{CO2}/g_{CaO} compared to the theoretical capacity of calcined dolomite ($CaO \cdot MgO$) of 0.46 $g_{CO2}/g_{CaO \cdot MgO}$ [18]. On the other side, dolomite has shown higher stability in sorption/desorption cycles than pure CaO [23].

In addition to an adequate sorbent, highly active and selective catalysts are required for producing high purity hydrogen from bio-oils reforming. Ni-based catalysts are widely employed in this

process due to their good balance between cost, activity and stability [15]. For this work Ni-based catalysts were prepared, with cobalt addition (which promotes C-C bond rupture [6]) and Pd addition (which can improve the stability of the catalyst decreasing the tendency of Ni to carbon formation [8,17,24]).

The main objective of this work was the development of different Ni-based catalysts, over conventional and non-conventional supports, to produce high purity hydrogen from sorption enhanced steam reforming of bio-oils. There is a lot of bibliography about acetic acid reforming, but our aim was to check how the prepared catalysts behave both with the acetic acid and with a more complex mixture. The effect of Co and Pd addition to the catalysts was tested, together with the effect of the feeding complexity, testing both the model compound acetic acid alone, and also a more complex mixture of compounds present in bio-oils, such as: acetic acid, acetone, phenol, furfural and 1-butanol. The obtained catalytic performance was discussed together with the characterization results, in order to better understand the activity and stability results. Another goal was to determine whether a rawer dolomite, and cheaper from a quarry close to us in Bilbao (Spain), could be employed as CO_2 sorbent.

2 Experimental procedure

2.1 Catalysts preparation

Three different catalyst types were prepared: Ni-based over a conventional support (γ-alumina), Ni-based over an unconventional support (olivine) and Ni-based hydrotalcite. Alumina and olivine catalysts were prepared by wet impregnation method. Olivine sand (48 wt% MgO, 41 wt% SiO_2 and 8 wt% Fe_2O_3) was provided by a casting company "Ilarduya y Cía". Prior to impregnation, supports were calcined at 700 ºC during 4 h in air, to minimize structural changes during the tests. With each support, three different catalysts were prepared: i) 40 wt% Ni, ii) 30 wt% Ni and 10 wt% Co, iii) 30 wt% Ni, 10 wt% Co and 1 wt% Pd. The metallic precursors employed were the following:

- Nickel (II) nitrate hexahydrated (99.999 wt% Sigma-Aldrich).
- Cobalt (II) chloride hexahydrated (98 wt% Sigma-Aldrich).
- Palladium (II) nitrate dehydrated (40% Pd basis, Sigma-Aldrich).

In order to get the desired composition of the catalysts, an appropriate amount of support and metallic precursors were mixed, with 10 mL of distilled water per gram of support. The suspension was mixed overnight. The excess of water was evaporated to dryness in a rotary evaporator (Heidolph Laborota 4000) at 45 ºC and vacuum. Once most of the solvent was evaporated, the resulting solid was introduced in an oven at 110 ºC during 12 h, to ensure complete drying. Then, the catalysts were calcined in air atmosphere at 700 ºC, with heating rate of 3 ºC/min, and keeping this temperature during 4 h. Finally, they were pressed and sieved in order to obtain a particle size of $0.42 < dp < 0.50$ mm. This particle size was selected with the aim of maintaining an internal pipe diameter-to-particle diameter higher than 10, to avoid reactants to bypass near the wall [25].

The Nickel hydrotalcite catalyst was prepared in the Norwegian University of Science and Technology by Prof. De Chen. It is prepared by co-precipitation of $Ni(NO_3)_2 \cdot 6H_2O$, $Mg(NO_3)_3 \cdot 6H_2O$ and $Al(NO_3)_3 \cdot 9H_2O$, and the nominal composition was 20 wt% Ni. Further explanations can be found in Fermoso et al. [26].

The prepared catalysts were named as follows: Ni/Al_2O_3, $NiCo/Al_2O_3$, $NiCoPd/Al_2O_3$, Ni/Olivine, NiCo/Olivine, NiCoPd/Olivine and Ni/HC.

2.2 CO_2 sorbents

Two dolomites from different quarries were employed as Ca precursors for CO_2 sorption. One of them, named as Norway Dolomite, was Artic dolomite and was supplied by Franefoss Miljøkalk A/S, Norway. According to the documentation provided by the supplier, its purity was approximately 98.5 wt% $CaMg(CO_3)$ and it had no sulphur according to X-ray fluorescence analysis [26]. The other dolomite, named as Castro Dolomite, was supplied by "Dolomitas del Norte" in Castrourdiales, Cantabria (Spain), part of the Calcinor group. Both dolomites were calcined in a muffle oven in air atmosphere at 700 ºC during 4 h before the sorption tests.

2.3 Characterization of sorbents and catalysts

Diverse characterization techniques were employed in order to determine the physicochemical properties of the fresh-reduced materials: inductively coupled plasma-optical emission spectroscopy (ICP-OES), CO chemisorption, N_2 adsorption-desorption isotherms, ammonia temperature-programmed desorption (NH_3 TPD), temperature-programmed reduction (TPR), X-ray diffraction (XRD), and X-ray photoelectron spectroscopy (XPS).

ICP-OES: With this technique, Ni, Co and Pd contents of the catalysts were determined. The solid samples were firstly disaggregated in acid solution (mixture of HF, HNO_3 and HCl) and then analysed in a Perkin-Elmer Optima 3300DV equipment.

N_2 adsorption-desorption: Textural properties of the catalysts, such as BET surface area, pore volume and average pore diameter were determined in an Autosorb 1C-TCD. Prior to the analysis, the samples were degassed at 300 ºC during 12 h. The surface area was calculated using the Brunauer-Emmett-Teller (BET) method, and pore size distribution is calculated using the Barrett-Joyner-Halenda (BJH) method.

CO chemisorption: The cumulative adsorbed CO, metal dispersion and active surface area of the previously reduced catalysts were determined by CO-pulse chemisorption in a Micromeritcs® AutoChem II. Samples were firstly reduced in a 5%H_2-Ar mixture at 700 ºC, and then CO chemisorption capacity was measured at 35 ºC in a 5%CO-He mixture till peaks were equal.

NH_3 TPD: Temperature programmed desorption of NH_3 was used in order to know the acid characteristics of the calcined and reduced samples. The employed equipment was a Micromeritcs® AutoChem II instrument. First of all, samples were reduced at 700 ºC in a 5%H_2-Ar mixture, then they were flushed by He for 30 min, followed by cooling at 100 °C and loading of NH_3 for 30 min. Then, the physically absorbed NH_3 was removed using He at 150 °C until no further desorption was recorded and release of chemically adsorbed NH_3 was collected increasing temperature from 150 °C to 895 °C at a rate of 10 °C/min.

TPR: The reducible species present in the calcined samples, and their reduction temperatures, were determined in a Micromeritcs® AutoChem II instrument. A continuous flow of 5%H_2-Ar (45 NmL/min) was passed over approximately 0.1 g of sieved sample. The temperature of the samples was increased from room temperature to 900 ºC at 1.2 ºC/min (the same heating rate employed during the activation of the catalyst in the bench-scale pilot plant prior to the experiments).

XRD: Crystalline species and approximation of the average crystal size (by Scherrer equation) of the reduced samples (at 700 ºC during 4 h) were calculated with the X-ray diffractograms obtained using a Seifert XRD 3000P diffractometer, equipped with a PWBragge-Brentano q/2q 2200 goniometer, bent graphite monochromator and automatic slit, using a Cu Kα radiation. XRD technique can measure around 1-2 μm depth of the sample.

XPS: Elemental composition at the catalysts' surface was determined with the XPS patterns of fresh-reduced catalysts in a SPECS (Berlin, Germany) system equipped with a Phoibos 150 1D-DLD analyser and an Al Kα (1486.6 V) monochromatic radiation source with electrons output angle of 90º. This technique can measure at about 10-20 nm depth of the sample, so compared to XRD it can be considered a surface analysis.

2.4 Fuel

Initially acetic acid was employed as a model compound of the organic acids present in the aqueous phase of bio-oils produced by the fast pyrolysis of biomass, which has being widely employed in the literature. The employed steam to carbon (S/C) ratio was 5 and the weight hour space velocity 0.8 $g_{reactants} \cdot g_{catalyst}^{-1} \cdot h^{-1}$. The prepared mixture for reforming had the following composition:

24.9 wt% acetic acid (Panreac 100%)
75.1 wt% distillate water

Secondly, a more complex mixture of model compounds was selected for reforming. The feeding mixture was fixed in order to keep the same moles of C fed per catalyst mass and time (0.0265 molC/($g_{cat} \cdot h$)) employed in the acetic acid tests. The carbon moles fed are directly proportional to the CO_2 produced, and therefore we could ensure that the maximum amount of CO_2 arriving to the sorbent in all the performed tests was the same. The specific composition of the employed mixture was decided taking into account the solubility of each compound and its relative presence in the bio-oils. Due to the different compounds employed, in the case of the complex mixture, the weight hour space velocity was 3.8 $g_{reactants} \cdot g_{catalyst}^{-1} \cdot h^{-1}$. In these reforming tests with complex mixture, higher S/C ratio was employed (S/C=7), trying to decrease the coke formation.

In all the cases the reactant liquid mixture was kept stirring during the tests, in order to ensure a homogeneous liquid mixture feeding to the reactor. The complex mixture had the following composition:

3.8 wt% acetic acid (Panreac 100%)
3.7 wt% acetone (Sigma-Aldrich ≥99.0%)
1.5 wt% phenol (Sigma- Aldrich ≥99.0%)
0.3 wt% furfural (Sigma-Aldrich 99.0%)
4.6 wt% 1-butanol (Sigma-Aldrich ≥99.7%)
86.1 wt% distillate water

The complete reforming reactions of the employed reactants are indicated below.

Acetic acid:	$C_2H_4O_2(g) + 2H_2O(g) \leftrightarrow 2CO_2(g) + 4H_2\ (g)$	ΔHº(25 ºC)=181 kJ/mol
Acetone:	$C_3H_6O(g) + 5H_2O(g) \leftrightarrow 3CO_2(g) + 8H_2$ (g)	ΔHº(25 ºC)=247 kJ/mol
Phenol:	$C_6H_6O(g) + 11H_2O(g) \leftrightarrow 6CO_2(g) + 14H_2\ (g)$	ΔHº(25 ºC)=395 kJ/mol
Furfural:	$C_5H_4O_2(g) + 8H_2O(g) \leftrightarrow 5CO_2(g) + 10H_2\ (g)$	ΔHº(25 ºC)=118 kJ/mol
1-butanol:	$C_4H_{10}O(g) + 7H_2O(g) \leftrightarrow 4CO_2(g) + 12H_2\ (g)$	ΔHº(25 ºC)=394 kJ/mol

2.5 Sorption enhanced steam reforming (SESR) experiments

SESR tests were performed in a bench-scale pilot plant (PID Eng&Tech) at atmospheric pressure. A schematic diagram of the experimental setup is shown in Figure 1. It consisted of a stainless steel fixed-bed reactor (8 mm internal diameter and 30 cm length) electrically heated in a furnace. The reactor temperature was controlled with a K-type thermocouple located in the catalyst/sorbent bed, just before the bed. The reactor was fed with 0.5 g of catalyst mixed with 2.5 g of dolomite. They were both fresh before each SESR test. The feeding gas flows were controlled with

Bronkhorst® mass flow controllers, and the aqueous solution was fed with a Gilson® HPLC pump. The liquid mixture was vaporized when entering to the reactor due to the high temperature. The effluent stream was cooled and condensed, and the gas phase was analysed online by a Varian MicroGC. The MicroGC was calibrated employing a standard gas mixture at periodic intervals. The flow rates of the outflow species (H_2, CO, CO_2, and CH_4) were estimated based on the nitrogen flow rate fed as the inert standard.

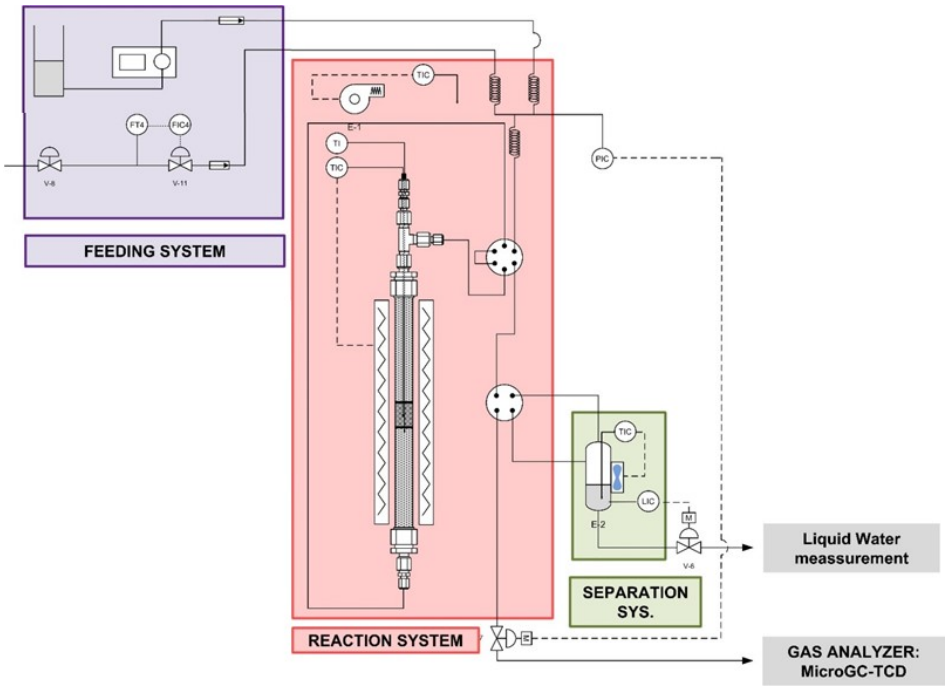

Figure 1. Diagram of the bench-scale pilot plant employed for the SESR tests.

Description of a typical operation procedure follows. The catalyst was firstly reduced at 700 ºC during 8 h, with a heating rate of 1 ºC/min, and 40 NmL/min of a N_2:H_2 1:1 mixture directly in the reactor. Then, the temperature was decreased to 575 ºC in nitrogen atmosphere, to purge the reactor, before starting the SESR tests. Once at 575 ºC, the liquid mixture plus 10 NmL/min of N_2, employed as internal standard, were fed to the reactor and the SESR test started. As soon as the dolomite was saturated with CO_2 the conventional SR took place, which was allowed to reach the steady state to compare the SR results with the SESR ones. After the composition of the reaction outflow was kept stable for around 30 min, desorption step was initiated. In order to desorb the CO_2, reactor temperature was increased until 750 ºC at 30 ºC/min under air atmosphere. In these conditions, the CO_2 could be desorbed and, if carbon deposition occurred during the SESR process, it could be burned and the catalyst and sorbent could be regenerated. Once all the CO_2 had been desorbed (when CO_2 was not detected in the outflow during around 15 min), the reactivation step started. In the reactivation step, temperature was decreased back to 575 ºC in N_2:H_2 1:1 mixture during 30 min. Then, hydrogen flow was stopped and only nitrogen was fed during 10 min, in order to be sure that all the hydrogen detected in SESR step was only the one produced in the reactions. The sorption and desorption cycles were repeated three times for each catalyst + sorbent mixture. After the third cycle, some tests were prolonged during around 48 h in order to analyse the stability of those catalysts in SR conditions.

During the SESR tests, H_2 yield (the produced hydrogen moles divided by the maximum hydrogen that could have been theoretically formed), selectivity to hydrogen (selectivity for hydrogen atoms to form molecular hydrogen instead of forming other hydrogen containing molecules, in our case only methane was detected) and H_2 purity in the outflow were calculated according to equations 1 and 2, respectively.

$$H_2 yield(\%) = 100 \cdot \left(\frac{F_{H2}}{4F_{Acetic\ acid} + 8F_{Acetone} + 14F_{phenol} + 10F_{furfural} + 12F_{butanol}} \right) \quad (1)$$

$$H_2 selectivity(\%) = 100 \cdot \left(\frac{2 \cdot y_{H2}}{2 \cdot y_{H2} + 4 \cdot y_{CH4}} \right) \quad (2)$$

Where, F_{H2} is the molar flow rate of the H_2 produced (mol/min), F_i is the molar flow rate of the *i* compound fed (mol/min), and y_{H2} and y_{CH4} are the produced molar fractions of H_2 and CH_4 respectively (N_2 free and on dry basis).

The carbon dioxide adsorbed before saturation of the dolomite was estimated in all the tests. The CO_2 concentration curve in the reactor outlet during the steam reforming was integrated and the CO_2 produced during the SESR was then subtracted.

3 Results and discussion

3.1 Characterization of sorbents

3.1.1 N_2 adsorption-desorption

In the current section, the surface structure of both Castro and Norway dolomites will be analysed with the N_2 adsorption-desorption data. In Table 1, a summary of the main structural information is given and the first critical difference between the dolomites is observed: the BET surface area. BET surface area is a method developed by Brunauer-Emmett-Teller to derive the surface area from physisorption isotherm data and is a simplification extension of the Langmuir mechanism to multilayer adsorption. Nevertheless, it is widely employed in sorbents characterization, and it will be employed here with comparison purpose. Sorption is a surface phenomenon, intensely affected by the surface area. Therefore, a high area is expected to have a positive effect on its sorption capacity. The surface area of the two dolomites is very different. In the work by Orio et al. they tested different quarries' dolomites and they also observed high variation in their surface structure [27].

Table 1. Structural properties of Norway and Castro dolomites.

	Norway Dolomite	Castro Dolomite
BET surface area (m^2/g)	39.1	0.09
BJH method cumulative desorption pore volume (cc/g)	0.1425	0.0039
BJH method desorption pore diameter (Å)	35	33

In Figure 2 the complete adsorption-desorption isotherms for both dolomites are given. Norway Dolomite corresponds to isotherm Type IV according to IUPAC classification of adsorption isotherms [28]. This sorption/desorption curve with hysteresis is typical in mesoporous solids. In this type of solids, sorption process is mainly determined by the sorbent-adsorbate interactions and by the condensate molecules interactions. The monolayer-multilayer initial sorption in the porous walls is followed by the condensation in the pores. When hysteresis appears is usually indicating that capillary condensation occurs in the pores. The interpretation of the sorption/desorption curve of Castro Dolomite was not reliable, due to a low surface area of the sample, and therefore the low accuracy of the measurement.

A B

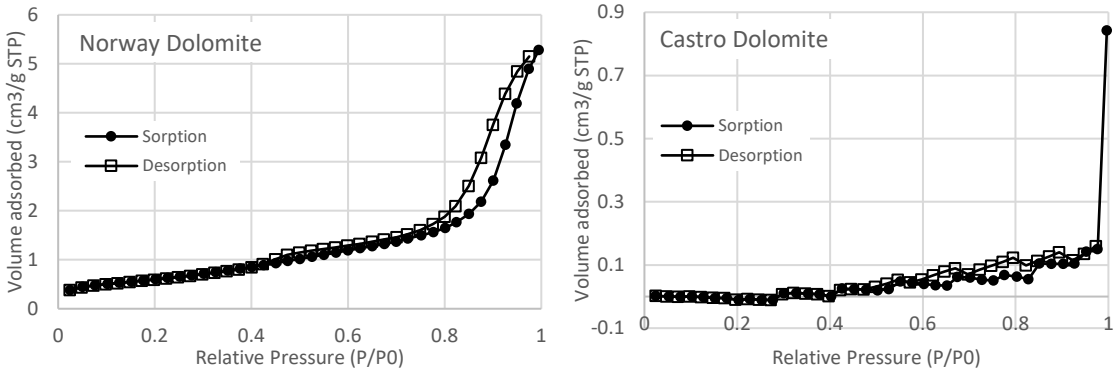

Figure 2. Adsorption isotherms for Norway (A) and Castro (B) dolomites.

As indicated before, analysing the isotherms both dolomites were mesoporous materials, but Norway Dolomite presented higher volume of pores. In addition, is also interesting to analyse the pore diameter distribution, as it strongly affects the sorption process of CO_2 on the sorbent surface. Furthermore, the solid $CaCO_3$ has around double specific molar volume than CaO [29]. Therefore, the particle porosity is reduced as sorption occurs, which can increase the pore diffusion resistance in the sorbent. Hu et al. showed in their work this pore change due to carbonation with SEM images in a Ca-based sorbent [30]. In Table 1, the average pore diameter estimated by BJH (Barrett-Joyner-Halenda) method is shown, which were similar for both dolomites. Additional pore diameter analysis can be done comparing the cumulative pore surface change at different pore diameters, shown in Figure 3 for diameters lower than 100 Å. From this plotting, it can be concluded that the Norway Dolomite presented a big amount of pores between 30 and 40 Å, which were the ones generating the high surface area.

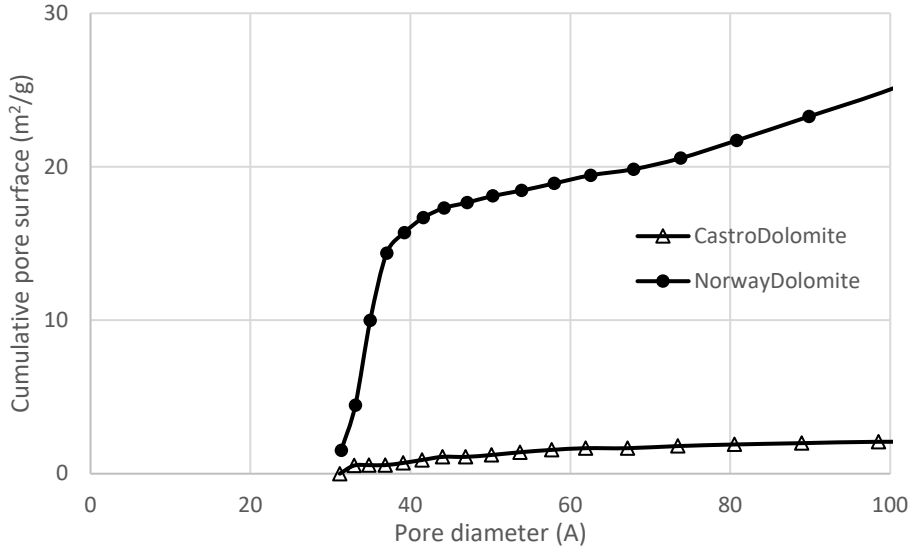

Figure 3. Cumulative surface area variation at pores lower than 100 Å for Norway and Castro dolomites (obtained from BJH desorption isotherms).

3.1.2 CO chemisorption

This technique is usually employed to analyse the metal dispersion of catalysts, but in the case of the sorbents it was just employed qualitatively, in order to check if there was a difference in the interaction of the dolomites and CO. The "CO adsorbed Cumulative Quantity" (CQ) of the two

dolomites is shown in Table 2. It can be observed that Norway Dolomite presented a higher interaction, which can be in accordance with its higher surface area (explained in previous section).

Table 2. CO chemisorption of the fresh-reduced two sorbents.

Sample	Adsorbed cumulative quantity (mol/g_{sample})
Castro Dolomite	0.00117
Norway Dolomite	0.00319

3.1.3 NH_3-TPD

The measured total acidity, by NH_3 desorption technique, of both Dolomites was very similar, 0.264 $mmol_{NH3}/g$ for Castro Dolomite and 0.269 $mmol_{NH3}/g$ for Norway Dolomite. Taking into account their high difference in surface area, similar acidity may indicate that Castro Dolomite was much more acid than Norway Dolomite.

3.1.4 TPR

Both sorbents showed an interaction with the hydrogen during the TPR test. As it can be observed in Figure 4, they showed an intense hydrogen consumption peak at around 600 ºC. There are no metals deposited over the sorbents, so the main objective of this technique with the dolomites is not to observe reduction peaks, but to analyse if the reduction step at 700 ºC employed in the bench-scale pilot plant prior to the experimental tests, could affect the behaviour of the sorbent. According to the obtained results, the Dolomites interacted with hydrogen in the temperature range of around 500-600 ºC. In the work by Taralas et al. [31] they observed two reduction peaks (at 622 ºC and 724 ºC) in a dolomite, which were related to MgO and to CaO because of independent crystals observed in SEM. In our case, we observed a single peak in the TPR. This may indicate that, in our case, the behaviour of CaO and MgO crystals is similar enough, regarding the effect of H_2, as to be detected as a single peak.

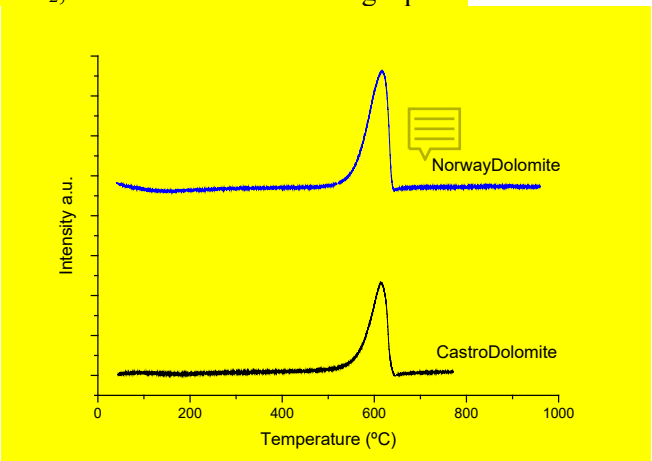

Figure 4. TPR peaks of Norway and Castro dolomites.

3.1.5 XRD

Norway and Castro reduced dolomites presented the same XRD pattern, as can be observed in Figure 5. In order to analyse the effect of the reduction step on dolomites, the Norway Dolomite

was also analysed fresh. The semi quantitative results of the four main components detected in the fresh sample are given in Table 3. The presence of portlandite ($Ca(OH_2)$) was due to the hygroscopic nature of the Ca-based materials [32]. During the reduction, most of the carbonates observed in the fresh sample were lost, as CO_2 most probably, and they were not detected in none of the reduced dolomites. After the reduction procedure, the magnesian calcite was reconverted mainly into CaO and MgO. This chemical change can be the one observed as a reduction peak in the TPR results at around 600 ºC.

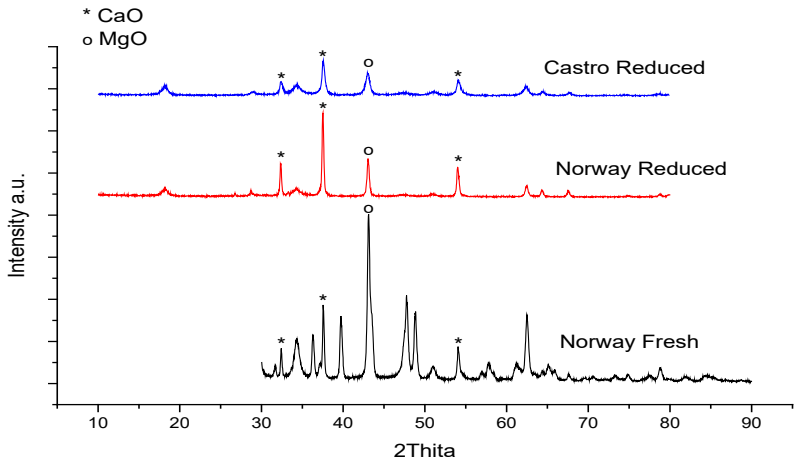

Figure 5. XRD diffractograms of the reduced Norway and Castro dolomites, together with the Norway fresh for comparison purpose.

Table 3. Semi quantitative XRD results for the fresh Norway Dolomite.

Calcite magnesian $(Mg_{0.064}Ca_{0.936})CO_3$	Lime CaO	Periclase MgO	Portlandite, syn $Ca(OH)_2$
59%	8%	25%	8%

3.2 Characterization of catalysts

3.2.1 ICP-OES

The content of nickel, cobalt and palladium in the tested catalysts is shown in Table 4. All the measures were repeated three times, with standard deviation lower than 0.5%. The nickel content was in all the catalysts, except in the $NiCO/Al_2O_3$ one, similar to the desired percentage. Cobalt and palladium percentages were in all the cases lower than the expected ones (10 wt% for Co and 1 wt% of Pd).

Table 4. Composition of the catalysts measured by ICP-OES.

Catalyst	wt% Ni	wt% Co	wt% Pd
Ni/Al_2O_3	41.34	-	-
$NiCo/Al_2O_3$	24.14	7.14	-
$NiCoPd/Al_2O_3$	29.92	8.76	0.85
Ni/Olivine	42.66	-	-
NiCo/Olivine	28.60	7.94	-
NiCoPd/Olivine	29.87	8.62	0.79
Ni/HC	19.8	-	-

3.2.2 N_2 adsorption-desorption

A general comparison of the catalysts' structure is given in Table 5. Alumina-based catalysts presented low BET surface area, as the metal content was high and it is known that high metal content blocks the surface. Olivine-based catalysts had a BET surface area of around 3-5 m^2/g, indicating a very low porosity. In the Ni/HC catalyst, it was noticeable the high BET surface area and the low BJH pore volume. This could be due to small pores in a narrow diameter range.

Table 5. Structural properties of fresh catalysts obtained by nitrogen sorption/desorption.

	BET surface area (m^2/g)	BJH pore volume (cc/g)	BJH average pore diameter (Å)
Ni/Al_2O_3	61	0.119	55
$NiCo/Al_2O_3$	45	0.114	56
$NiCoPd/Al_2O_3$	41	0.103	58
Ni/Olivine	5	0.015	31
NiCo/Olivine	3	0.005	31
NiCoPd/Olivine	4	0.016	35
Ni/HC	151	0.047	37

The complete nitrogen sorption/desorption isotherms are shown in Figure 6. If comparing these isotherms with the IUPAC nomenclature, it is observed that alumina-based catalysts can be identified as Type IV(a) with hysteresis, representing mesoporous materials with initial sorption of monolayer-multilayer in the surface followed by capillary condensation in the meso pores. In the case of olivine-based catalysts, they presented a very small, or not noticeable, hysteresis; and they can be associated with Type III isotherms, which are reversible isotherms. This isotherm indicates that there is not monolayer formation. The interactions between the adsorbed molecules with the sorbent are weak, and the molecules are grouped together in more favoured active sites of the solid surface, which can be considered almost non porous. Ni/HC catalyst showed a small hysteresis with higher increase of adsorbed volume rate at lower relative pressures, which usually indicates sorbent-adsorbate interactions in narrow micropores. Comparing for all the catalysts the rate at low relative pressures, it can be concluded that Ni/HC was the only one presenting this; indicating the presence of narrower pores' diameter or more small pores. This conclusion is in agreement with the one reached in Table 5. The Ni/HC catalyst showed also a small hysteresis, indicating also some capillary condensation.

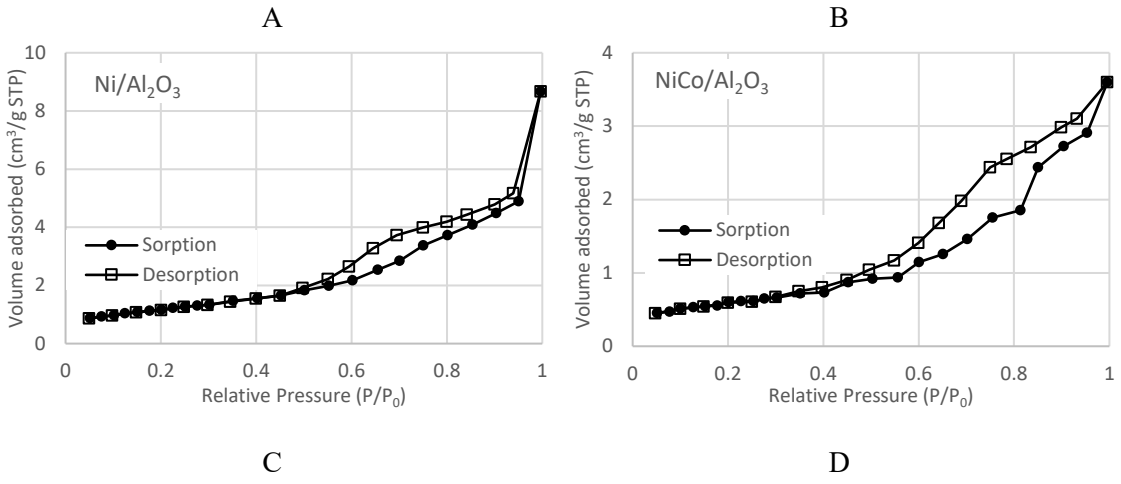

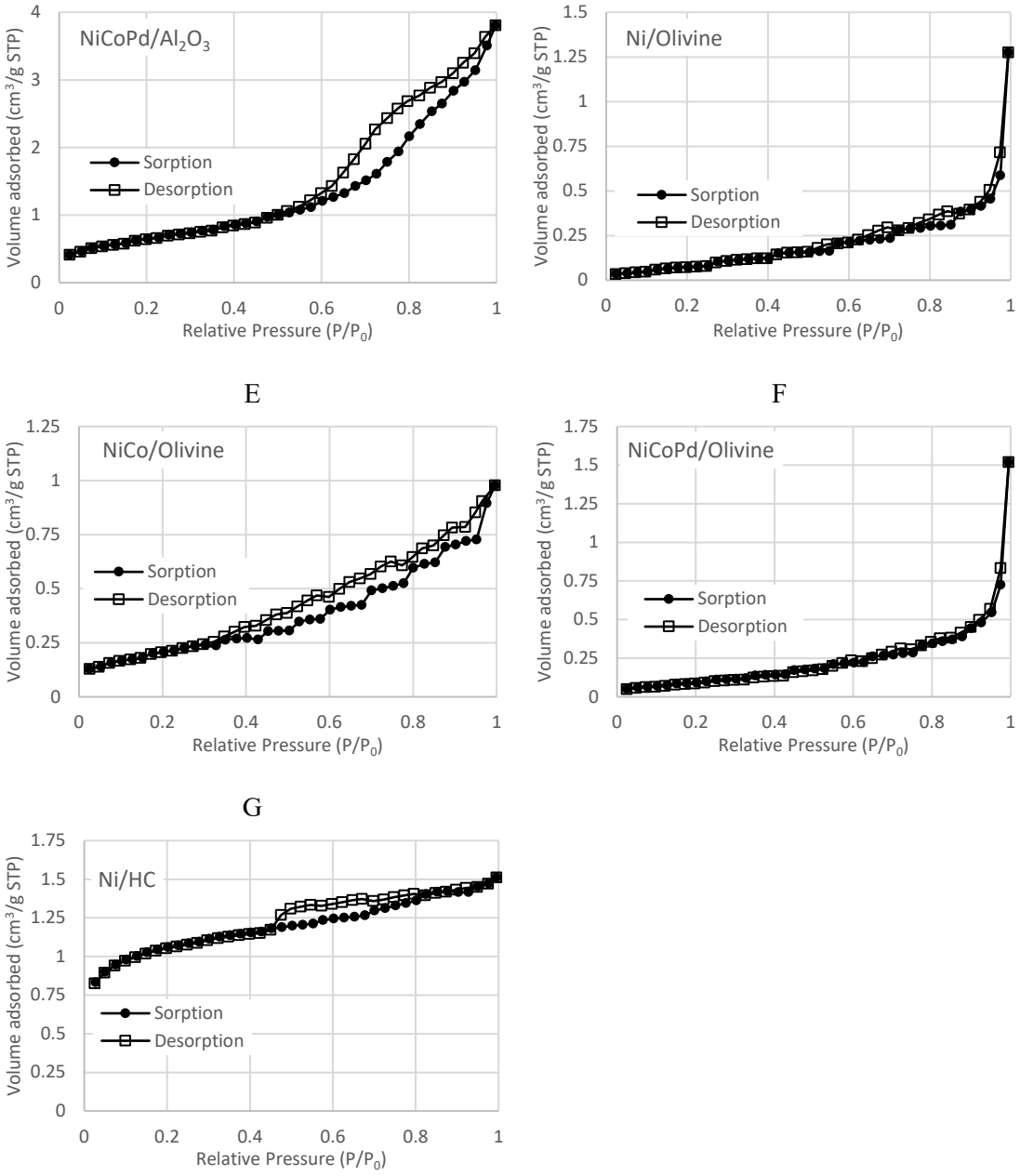

Figure 6. Nitrogen sorption/desorption isotherms for the tested catalysts.

In Figure 7, the cumulative pore surface of the tested catalysts is shown for pore diameters lower than 100 Å. All the catalysts were mesoporous/macroporous materials, with pore diameters starting at around 30 Å. In the alumina and olivine-based catalysts, the addition of cobalt decreased the surface area, and the addition of both Co and Pd decreased even more the surface; indicating that the metal deposition blocked pores in the entire range of diameters. As it has been previously indicated, in general, olivine-based catalysts presented lower surface area than the rest, but the pore diameters were similar. Regarding the Ni/HC catalyst, an important difference was observed in the figure; pores in the range of 35-40 Å give most of the surface area, which indicates a very homogeneous porosity structure.

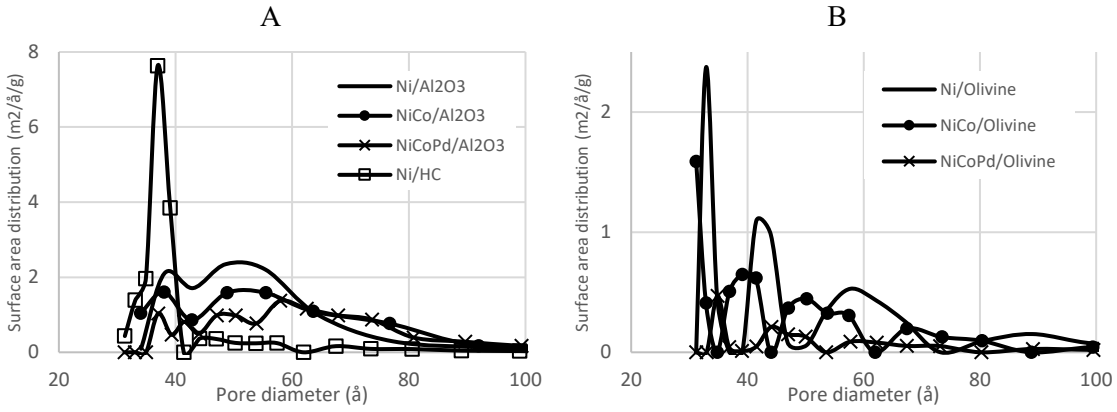

Figure 7. Cumulative pore surface distribution as a function of pore diameter for the tested catalysts.

3.2.3 CO chemisorption

The "Active Metal Surface Area" (AMSA) and the "Metal Dispersion" (MD) were determined by pulse CO chemisorption, and the results for all the catalysts are shown in Table 6. The comparison of the AMSA and MD values for the catalysts with more than one metal are descriptive, because it is difficult to attribute each result to the interaction of each metal. In the case of the monometallic catalysts (41 wt% Ni/Al_2O_3, 43 wt% Ni/Olivine and 20 wt% Ni/HC), the dispersion of Ni over alumina was much higher than over olivine, even though they had similar Ni weight percentage. Ni/HC catalyst showed the best dispersion, indicating a small Ni size in the catalyst. Comparing the monometallic and the bimetallic catalysts of alumina and olivine, the dispersion seemed to be better in the bimetallic ones. However, looking at the "CO adsorbed Cumulative Quantity" (CQ), it is concluded that the adsorbed CO quantity was almost the same for both. This can be due to a smaller total metal weight in the case of the bimetallic, and may be an indication of a different deposition behaviour of Ni and Co. Regarding the trimetallic catalysts, in the case of the alumina-based catalyst the CQ was almost half of the other two alumina catalysts. The trimetallic olivine-based catalyst showed higher CO sorption than the monometallic and bimetallic, but in all the cases the values were very small.

Table 6. CO chemisorption of the fresh-reduced catalysts.

Sample	Active metal surface area (m^2/g_{sample})	Metal dispersion (%)	Cumulative quantity (mol/g_{sample})
Ni/Al_2O_3	0.6534	0.2376	0.01672
$NiCo/Al_2O_3$	0.6529	0.3131	0.01663
$NiCoPd/ Al_2O_3$	0.3108	0.1185	0.00790
Ni/Olivine	0.0095	0.0033	0.00024
NiCo/Olivine	0.0114	0.0047	0.00029
NiCoPd/Olivine	0.0199	0.0076	0.00051
Ni/HC	2.7142	2.0588	0.06943

3.2.4 NH_3-TPD

The measured total acidity, by NH_3 sorption technique, of all the catalysts is shown in Table 7. As expected, olivine-based catalysts showed no acidity, whereas the highest value was detected for the Ni/HC one. A higher acidity is expected to produce better C-C and C-O binding breakings, and higher coke formation during the reforming reactions [8,9].

Table 7. Total acidity ($mmol_{NH3}/g$) of the catalysts measured by NH_3 sorption technique at temperatures lower than 890 ºC.

Ni/Al_2O_3	$NiCo/Al_2O_3$	$NiCoPd/Al_2O_3$	Ni/Olivine	NiCo/Olivine	NiCoPd/Olivine	Ni/HC
0.32	0.23	0.20	n.d.	n.d.	n.d.	0.37

n.d.: not detected

3.2.5 TPR

In order to analyse the reduction properties of the tested catalysts, TPR analysis were performed with small heating rate, 1.2 ºC/min (the same one employed in the reduction step in the bench-scale pilot plant tests). In Figure 8, the temperature reduction peaks of the catalysts are shown. In the alumina catalysts a main reduction peak at around 300 ºC was observed, slightly shifted to smaller temperatures with the addition of Co and Pd. This may be due to an easier reduction behaviour due to the addition of Co and Pd. Another small reduction area can be observed at temperatures higher than 700 ºC, which may indicate that the reduction of some atoms is high energy demanding, due to stronger interaction with the support.
In the olivine catalysts, wide reduction temperature range was observed. The trimetallic olivine catalyst seemed to be completely reduced at lower temperature than the other two olivine catalysts, which may strength the idea of Pd improving the reducibility of the metals. Finally, the Ni/HC catalyst showed that reduction started already at around 200 ºC, with a peak at 300 ºC. These low reduction temperatures are in accordance with the high Ni dispersion observed by CO-chemisorption and the small crystal particle size identified by XRD. Smaller Ni particles are easier to reduce. The reduction of the catalyst seems to continue until temperatures as high as 600 ºC. Therefore, Ni/HC catalyst presented some Ni particles weakly interacting with the support and others with high interaction that make them more difficult to reduce, which was also observed by Wierzbicki et al. [33].

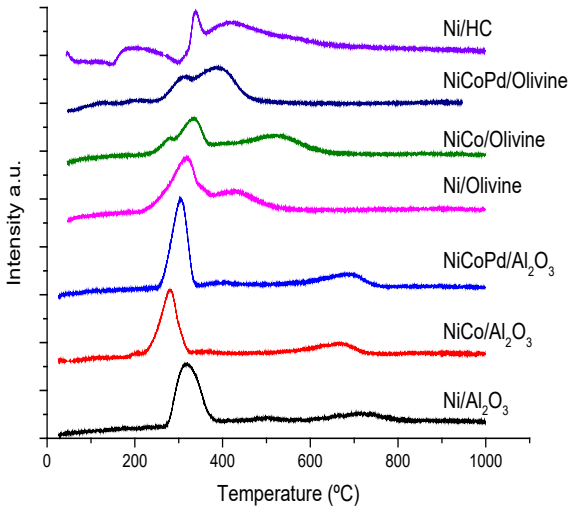

Figure 8. TPR peaks of the catalysts.

3.2.6 XRD

A fresh-reduced sample of all the catalysts was analysed by XRD (see Figure 9). The three most characteristic peaks of metallic nickel (01-087-0712, indicated with *) were clearly detected in all the samples except in the Ni/HC. In this catalyst, the peaks at 2Theta values of 44.7 and 52 were less intense and broader, indicating that the crystals seemed to be smaller. Cobalt and palladium crystallites were not detected by XRD in the samples. Metallic nickel and cobalt have a very similar diffractogram. Therefore, nickel had most probably masked the cobalt signs and it made it hard to distinguish from each other [6]. Palladium was most probably in small amount or small crystals (< 1 nm) as to any diffraction peak be detected. In the olivine-based catalysts signals of olivine (Mg_2SiO_4, 01-084-1402) can be observed all along the diffractogram.
With Scherrer equation the crystallites size can be estimated. Nickel crystal's size was calculated for all the catalysts with the peak at 44.7. Alumina-based catalysts had an average size of 120 nm, the olivine-based catalysts 150 nm and the Ni/HC 10 nm. These values were in accordance with the qualitative results obtained from CO-Chemisorption, where the active metal surface was the highest in Ni/HC and the smallest in the Ni/Olivine.

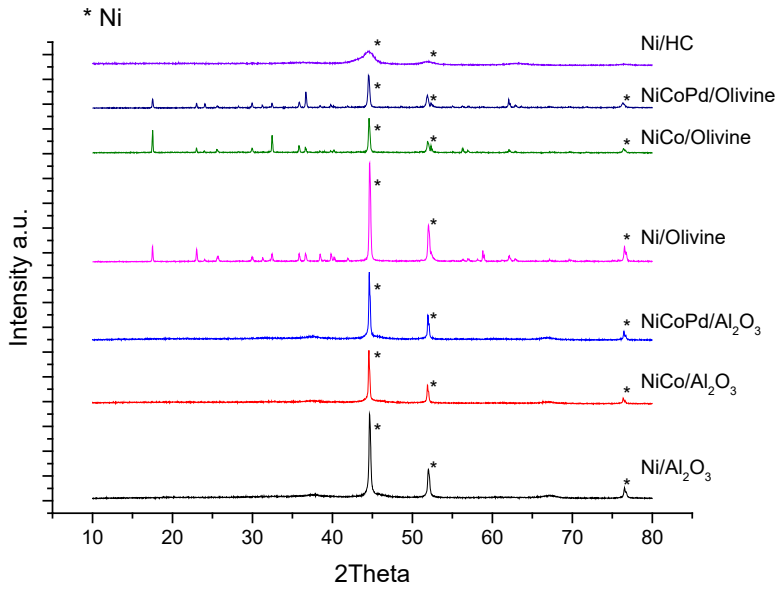

Figure 9. XRD diffractograms of the fresh-reduced catalysts samples.

3.2.7 XPS

Fresh and reduced catalysts were analysed by XPS. This technique allows to examine the surface composition and to identify the chemical nature of the elements present there. All the samples showed elemental carbon in the surface, which was most probably due to pollution from atmospheric contamination during the handling of the sample. This carbon percentage on the surface depended on the material, and olivine samples presented higher amount than alumina or HC. A summary of the main results is given in Table 8. In the catalysts containing cobalt, its presence was observed, but it could not be quantified due to superposition with the LMM Auger line of Nickel. In Olivine catalysts, Si and Mg were identified on the surface and Al and Mg were detected in Ni/HC, as expected from their composition and preparation method.

Table 8. Relative atomic composition and atomic Al/O ratio of the fresh and reduced catalysts by XPS analysis.

	Al/O atomic ratio	Relative at% Ni
Ni/Al_2O_3	0.54	10.1
$NiCo/Al_2O_3$	0.47	6.4
$NiCoPd/Al_2O_3$	0.50	7.0
Ni/Olivine	-	8.6
NiCo/Olivine	-	4.5
NiCoPd/Olivine	-	7.4
Ni/HC	-	1.6

In Figure 10, it is shown the XPS results of the fresh and reduced catalysts for the Nickel binding energy range. The main nickel specie detected in all the samples was Ni^{2+} as nickel oxide (853.8-854.3 eV in the literature) with its corresponding satellite peak (~860 eV). The binding energy of Ni^0 is referenced at around 852.7-852.8 eV (Ni 2p 3/2), which is not usually observed in samples exposed to air due to passivation layer. In the three alumina-based catalysts, the atomic ratio Al/O was higher than that in alumina (Al/O=0.666). The surface of these catalysts had more oxygen than that coming from alumina, indicating a quick superficial reoxidation of Ni during the handling of the samples. Most probably, Ni was oxidized in all the catalysts, but it is not possible to check this comparing the atomic ratios due to the complexity of the Olivine and HC supports. The peaks observed at around 870-880 eV are from Ni 2p 1/2 and its corresponding satellite peak. The quick reoxidation of the catalysts made necessary the re-activation step between sorption cycles performed during the SESR tests, and explained in section 2.5.

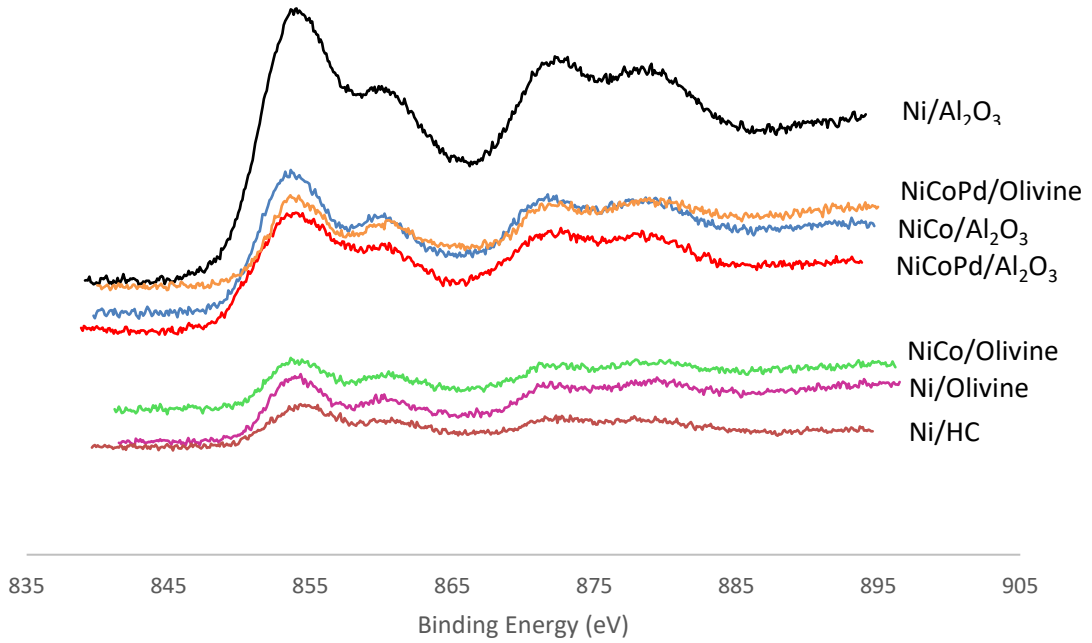

Figure 10. XPS peaks of fresh and reduced catalysts for the binding energy range of Nickel.

3.3 Sorption enhanced steam reforming experiments with acetic acid

3.3.1 SESR operating conditions optimization

Before the SESR tests for catalysts performance comparison, several operation parameters were

optimized. First of all, the two available dolomites were compared in SESR operating conditions. Previously from the characterization results, mainly in the N_2 sorption/desorption isotherms, it has been concluded that Norway dolomite presented surface characteristic that could foresee a better sorption capacity. This was also corroborate with SESR tests. In Figure 11 it can be observed the sorption capacity of both dolomites at the same conditions, in all the cases Norway Dolomite presented higher sorption capacity. Therefore, all the SESR tests were performed just with Norway Dolomite.

The second parameter to be optimized was the heating rate employed during the activation step prior to SESR tests (700 ºC under H_2:N_2 atmosphere, further details in section 2.5). In the quick activation procedure (Figure 11A) a heating rate of 5 ºC/min was employed, whereas in the slow activation procedure (Figure 11B) the heating rate was 1 ºC/min. It can be concluded from the figures that a high heating rate until 700 ºC seemed to damage or modify the sorbents, obtaining less sorption capacity for both dolomites. As a conclusion, in all the SESR performed to compare the catalysts behaviour, low activation rate was employed.

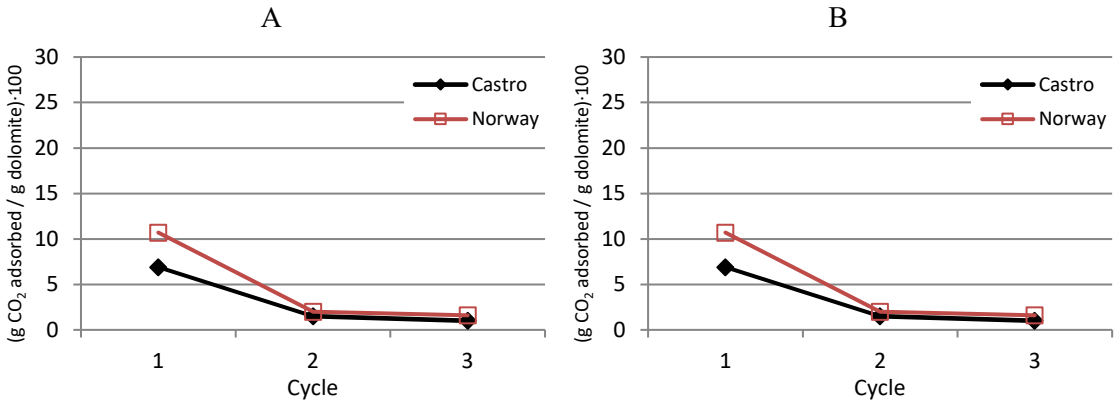

Figure 11. The CO_2 sorption capacity of Norway and Castro dolomites during three cycles at SESR conditions. A: quick activation, B: with slow activation.

Another two operation parameters were optimized to allow enough time before breakthrough curve with the less amount of sorbent involved. Two different feeding space velocities were analysed (0.8 and 1.6 h^{-1}) and better sorption capacity was observed with the lowest velocity, as observed in Figure 12A. This indicated that there were not external mass transfer limitations when operating with the low space velocity, and that in the high space velocity test the sorption capacity was limited by the CO_2 space velocity in the bed.
In Figure 12B, the employed sorbent weight effect was analysed. The sorbent weight to be employed was mainly limited by the available sample and the reactor internal volume. Similar sorption capacities were measured with enough breakthrough time for both 2.5 and 5 g of sorbent; therefore, it was decided to employ 2.5 g in all the SESR tests performed for catalysts' comparison.

A B

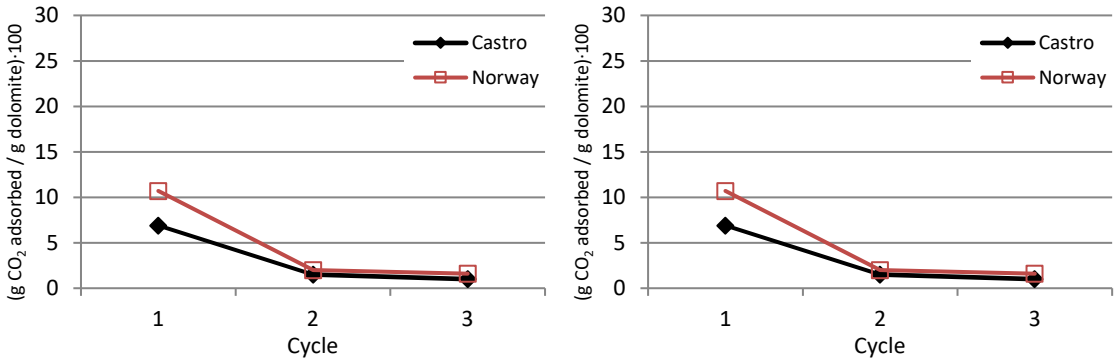

Figure 12. Effect of some operation parameters on the sorption capacity of Norway Dolomite. A: the effect of weight hour space velocity; B: the effect of sorbent amount.

3.4 Thermodynamic analysis

Employing Aspen Plus software, a thermodynamic analysis was performed with a theoretical RGibbs reactor that uses Gibbs free energy minimization to calculate equilibrium. The reforming of the two mixtures employed in the SESR experimental tests (acetic acid AA + water and complex mixture CM + water) were simulated at the conditions employed in the experimental bench-scale pilot plant, at 575 ºC and 1 atm. The thermodynamic results obtained were compared with the experimental results from NiCoPd/Olivine (see Table 10). The experimentally yielded concentrations are divided into two columns, the period where the sorbent was shifting the reaction (SESR) and once the sorbent was saturated and we only have the SR process.

In the theoretical results, it was observed that the hydrogen production can be higher when reforming the complex mixture, generating higher concentration of hydrogen (70.96%). With both feedings, AA and CM, the reforming seemed to be almost complete, because the production of CO was quite low, and there was almost no methane. Comparing the theoretical SR with the experimentally obtained values, it can be easily observed that the complex mixture was more difficult than acetic acid to be reformed, as the difference between theoretical and experimental was higher with CM. Regarding selectivity, CO generation was not detected experimentally, which was a very interesting result; whereas there was more methane than the thermodynamic maximum expected. This can be an indication of good selectivity of the employed catalysts for feeding reforming, and also to the presence of some methanation side reaction ($CO_2 + 4H_2 \leftrightarrow CH_4 + 2H_2O$).

During the experimental SESR period, before reaching sorbent saturation, the equilibrium shift was easily observed both in hydrogen purity and in the generation of products from secondary reactions. Hydrogen purity reached values around 97%, which was very promising for being directly employed as a hydrogen current, with no presence of CO (critical compound for being employed in fuel cells, for example). Methane generation was much smaller than in reforming, indicating also the diminution of secondary reactions even in the hardest reforming conditions with CM feeding.

Table 9. Comparison of thermodynamic results obtained for acetic acid (AA) and complex mixture (CM) reforming compared with the experimental SESR and SR ones.

	Theoretical SR		Experimental SESR		Experimental SR	
mol%	AA	CM	AA	CM	AA	CM
H_2	64.87	70.96	97.03	97.40	61.73	65.26
CO	4.32	3.52	0.00	0.00	0.00	0.00
CO_2	30.54	25.25	0.06	2.57	34.03	30.83
CH_4	0.27	0.27	2.91	0.03	4.24	3.91

Ethane	0.00	0.00	0.00	0.00	0.00	0.00

3.4.1 SESR tests with acetic acid

All the catalysts were tested for acetic acid reforming under the following conditions: slow activation heating rate (1 ºC/min), 2.5 g of Norway Dolomite, 0.5 g of catalyst and weight hour space velocity of 0.8 h^{-1}. Three sorption/desorption cycles were performed with all the catalysts. The catalytic performance (hydrogen purity, selectivity and yield) obtained for the seven catalysts is shown in Figure 13, Figure 14 and Figure 15. In Figure 13 it is remarkable the high hydrogen purity obtained during the SESR, around 96.5 and 99.7%. The breakthrough curve was also observed as hydrogen purity during the SESR period was very close to 100%, while it quickly decreased to 55-60% when the sorbent started to be saturated. The sorption capacity of the sorbent, in all these tests, was much higher in the first cycle than in the second and third, which was easily observed with the shorter time at which hydrogen purity was close to 100%.
Regarding the alumina-based catalysts, they all showed similar behaviour during the SESR period, but after the sorbent reached saturation the hydrogen purity obtained with the Ni one was lower than that obtained with Co and CoPd addition. This difference was almost no noticeable in the olivine-based catalysts. This was an interesting result, taking into account that heterogeneous catalysis is a surface process, and the low BET surface area of the olivine-based catalysts. Concerning the Ni/HC catalyst, its activity was very similar to the other ones. However, is worth mentioning that its nickel content was around half of the other catalysts. It is also important to highlight that all the catalysts seemed to be stable, during the tested three cycles, as they all presented same results in the SR conditions (after sorbent saturation).

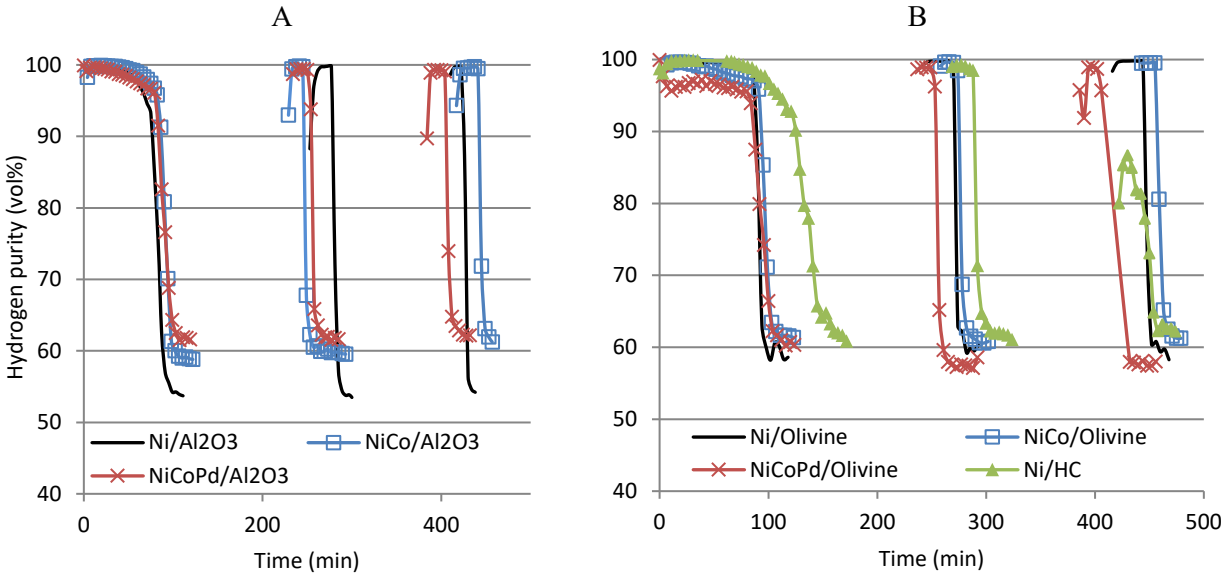

Figure 13. Hydrogen purity obtained during the three acetic acid SESR cycles performed with the tested catalysts. A: Alumina-based catalysts; B: Olivine-based catalysts and Ni/HC.

Hydrogen selectivity (see Figure 14) was calculated taking into account the selectivity for hydrogen atoms to form molecular hydrogen instead of forming other hydrogen containing molecules. It was observed that during the SESR period almost all the hydrogen atoms were employed for generating only hydrogen. This is a good indication of the equilibrium shift to hydrogen production due to CO_2 sorption, decreasing the secondary reactions. When the sorbent reached saturation, only CH_4 was detected as hydrogen containing other molecule. It is also

remarkable that CO was not detected during the experiments, a signal of good selectivity of the catalysts for the main hydrogen production reaction and an indication of no Water Gas Shift reaction occurring in the system ($CO + H_2O \leftrightarrow H_2 + CO_2$). In the alumina-based catalysts, the Ni one presented again worst behaviour than the Co and CoPd ones. In fact, Ni/Al_2O_3 was the one with the lowest selectivity among all the tested catalysts. It is worth mentioning the improving selectivity of Ni/HC observed along the three sorption cycles, changing from 76 to 95%.

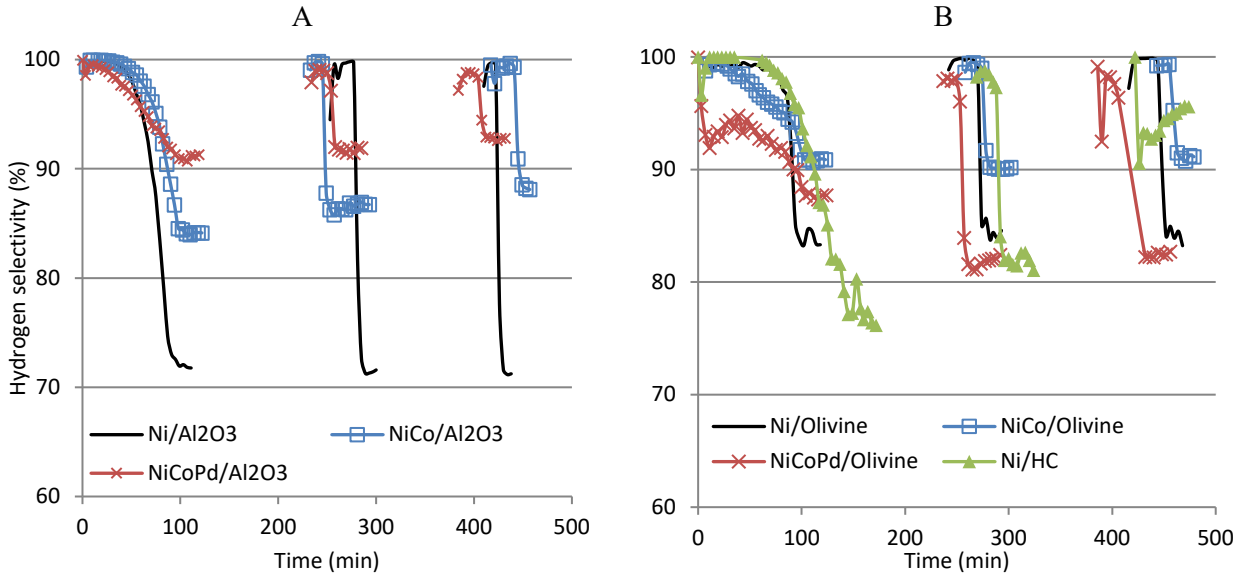

Figure 14. Hydrogen selectivity obtained during the three acetic acid SESR cycles performed with the tested catalysts. A: Alumina-based catalysts; B: Olivine-based catalysts and Ni/HC.

When comparing the hydrogen yield (the produced hydrogen moles divided by the maximum hydrogen that could have been theoretically formed) for the seven catalysts, see Figure 15, the effect of SESR period was less obvious than in the hydrogen purity and selectivity. Again, a positive effect of Co and Pd addition to alumina-based catalysts was observed, whereas it was not so remarkable in the case of olivine-based ones.

In Table 11, the sorption capacity of the Norway Dolomite during the acetic acid tests is shown. As it can be observed, it was not strongly affected by the small variations of gas composition and CO_2 production that could derive from the performance variations of each catalyst. In all the cases, the sorption capacity showed a high decrease from cycle 1 to 2, indicating that the sorption process was not totally reversible, or that the desorption step was slower than expected and the complete desorption of CO_2 was not achieved between cycles. The sorption capacity was kept much more constant for the forthcoming cycles, but in values lower than those previously reported for similar sorbents. The decrease in the CO_2 sorption capacity with cycles has being previously observed, and can be attributed to thermal sintering (the Tammann temperature of $CaCO_3$ is 533 ºC), resulting in the destruction of pore volume [32].

Table 10. Sorption capacity (g CO_2 adsorbed/g dolomite)·100 of the Norway dolomite recorded in the SESR cycles of acetic acid performed with each catalyst.

	Cycle 1	Cycle 2	Cycle 3
Ni/Al_2O_3	23.9	6.1	5.5
$NiCo/Al_2O_3$	28.5	5.2	6.3

$NiCoPd/Al_2O_3$	29.5	7.4	7.1
Ni/Olivine	26.7	8.5	9.3
NiCo/Olivine	30.5	6.1	6.8
NiCoPd/Olivine	27.9	6.3	5.2
Ni/HC	21.9	5	3.1

3.5 SESR with the complex mixture

All the catalysts were also tested for complex mixture reforming under the following conditions: slow activation heating rate (1 ºC/min), 2.5 g of Norway Dolomite, 0.5 g of catalyst and weight hour space velocity of 3.8 h^{-1}. Three sorption/desorption cycles were performed with each catalyst and their catalytic performance (hydrogen purity, selectivity and yield) is shown in Figure 15 and Figure 16. Analysing the hydrogen purity (see Figure 15) it can be observed that during the first SESR period, before the breakthrough curve, very high purities were obtained again for all the catalysts, 97-99%. It is a very interesting result to obtain such a high hydrogen purity even though the mixture is much more complex to reformate than the acetic acid. Once the sorbent was saturated, when conventional steam reforming took place, the hydrogen purity was very similar for all the tested catalysts, and higher than the one obtained in the acetic acid reforming (55-62%, see Figure 13). This indicated that the prepared catalysts were very adequate for the reforming of the complex mixture. The addition of Co and Pd did not show a clear improve in the catalytic behaviour at the tested conditions.

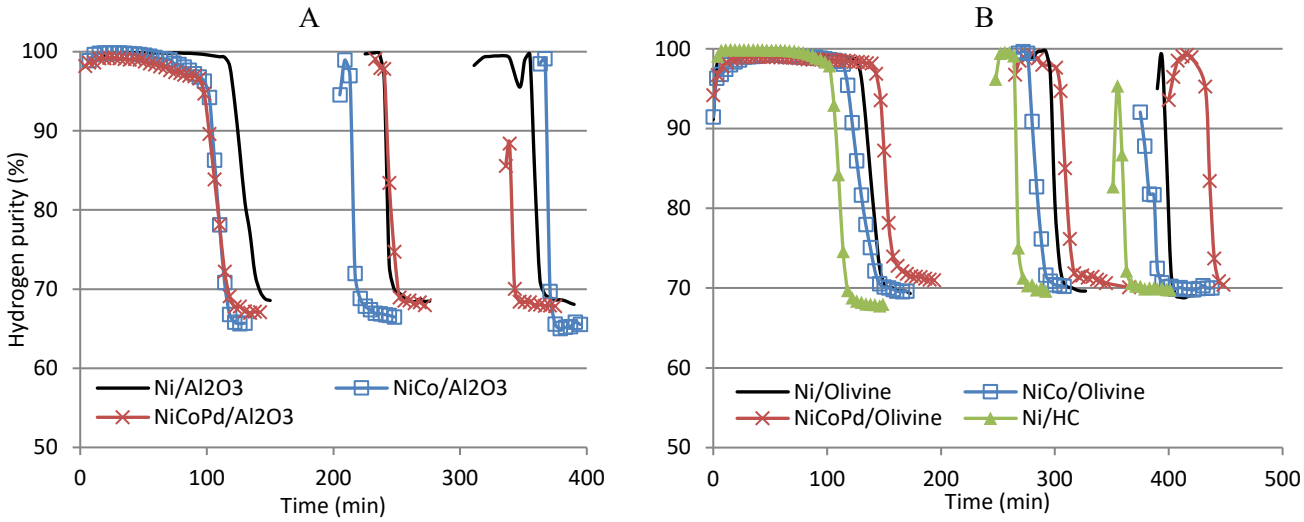

Figure 15. Hydrogen purity obtained during the three complex mixture SESR cycles performed with the tested catalysts. A: Alumina-based catalysts; B: Olivine-based catalysts and Ni/HC.

The hydrogen selectivity was higher than when reforming acetic acid, indicating that hydrogen atoms had a higher tendency to form hydrogen than other hydrogen containing molecules. In fact, the only hydrogen-containing molecule detected, different from molecular hydrogen, was again methane. What is worth mentioning in this case, is the smaller effect of equilibrium shift due to sorption detected in all these three cycles, compared to the acetic acid results. During the first cycle was possible to see the positive effect of sorption in selectivity, but during second and third the effect was almost negligible.

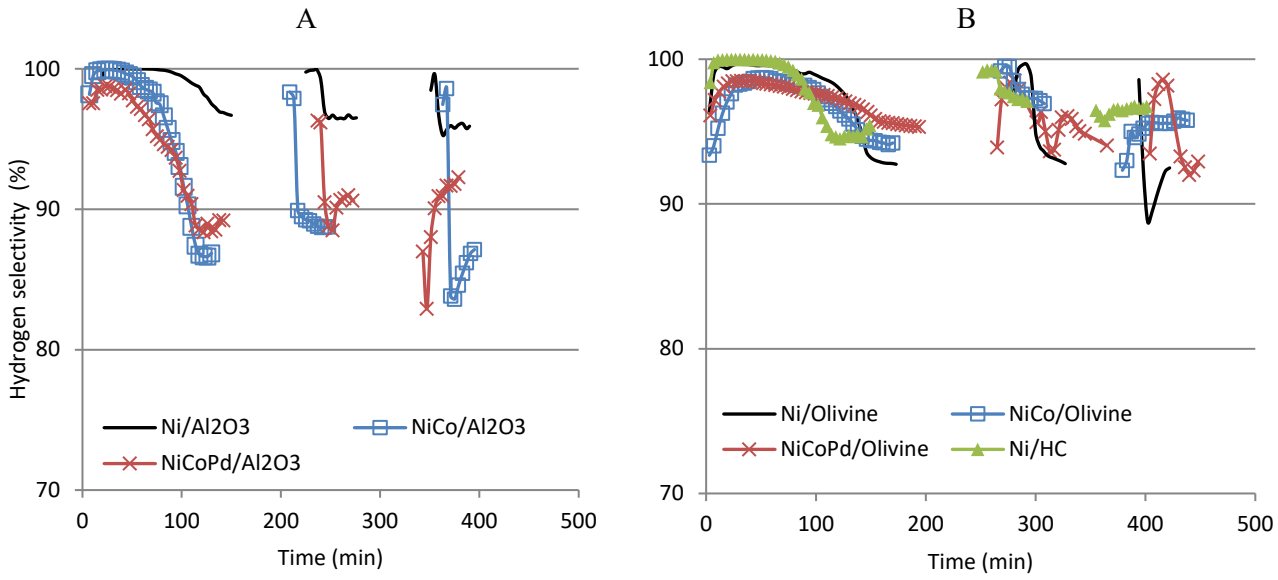

Figure 16. Hydrogen selectivity obtained during the three complex mixture SESR cycles performed with the tested catalysts. A: Alumina-based catalysts; B: Olivine-based catalysts and Ni/HC.

In Table 13, it is shown the CO_2 amount adsorbed by the dolomite during the complex mixture reforming. The sorption capacity calculated during the first cycle was in the range of the ones calculated during acetic acid reforming (23-30 ($g_{CO2\ adsorbed}/g_{dolomite}$)·100). Again, the capacity strongly decreased from the first to the second cycle, and also this time from the second to the third. Comparing the capacity decrease detected when reforming acetic acid and complex mixture it can be easily concluded that in the case of the complex mixture the sorption capacity was negatively affected. Most probably there was more coke generated, which was not removed during the oxidation step between SESR cycles, or maybe there were some by-products blocking the surface of the sorbent. The small sorption capacities of the second and third cycles were the reason for so short SESR periods observed during the tests and discussed before in the catalytic activity analysis.

Table 11. Sorption capacity (g CO_2 adsorbed/g dolomite)·100 of the Norway dolomite recorded in the SESR of mixture cycles performed with each catalyst.

	Cycle 1	Cycle 2	Cycle 3
Ni/Al_2O_3	23.6	4.2	1.3
$NiCo/Al_2O_3$	27.8	1.8	1.9
$NiCoPd/Al_2O_3$	25	2	0.8
Ni/Olivine	29.9	4.4	1.2
NiCo/Olivine	29	3.7	1.2
NiCoPd/Olivine	25.1	1.6	1.1
Ni/HC	28.4	4.1	1.2

3.6 SR stability tests

Some of the tested catalysts were kept under steam reforming conditions for longer time, in order to have some information about their stability. Reforming of acetic acid was maintained for three catalysts: Ni/Al_2O_3, Ni/Olivine and NiCo/Olivine (see Figure 17) and the mixture reforming conditions for the NiCo/Olivine catalyst (see Figure 18). During the tested time they all remained

very stable, indicating that they were not deactivated. The best hydrogen yield was obtained for the NiCo/Olivine catalyst and it was very similar for both feedings, 70-80% for acetic acid and 70% for complex mixture. The good stability of this catalyst can be related with its low acidity, avoiding coke deposition and therefore deactivation.

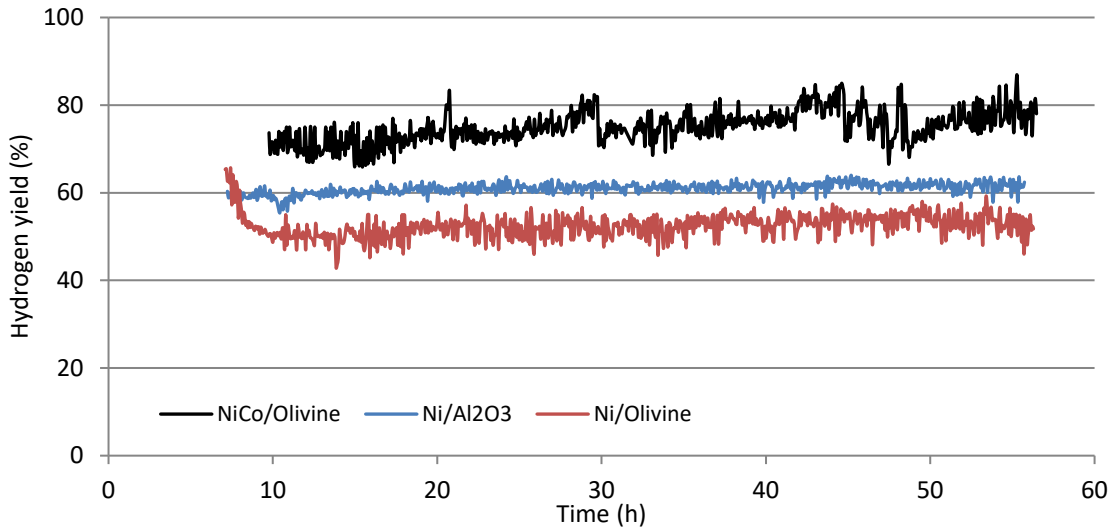

Figure 17. Hydrogen yield obtained during the stability test with acetic acid steam reforming with three catalysts.

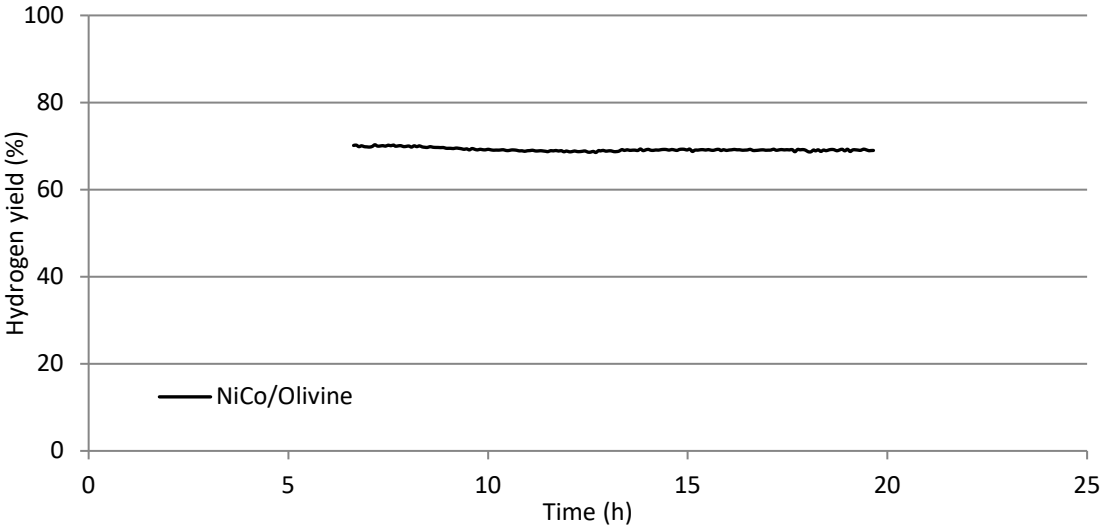

Figure 18. Hydrogen yield obtained during the complex mixture steam reforming stability test with NiCo/Olivine catalyst.

4 Conclusions

Between the two tested dolomites, the Norway Dolomite showed much better sorption properties than the Castro one. Both presented similar behaviour during the reduction step in the bench-scale pilot plan and they were both mesoporous materials, but the Norway Dolomite had much higher pore volume. During the characterization performed to the catalysts employing different

techniques, it was observed that Ni/HC catalyst presented much higher surface area with small pore diameter range, and smaller metal particle size than the rest of the catalysts. Significant catalytic differences were not detected by the addition of Co or Pd to the Ni-based catalysts. Ni/HC catalyst showed comparable catalytic behaviour, despite the fact that it contained half of the metal quantity than the others. In the steam reforming stability tests it was observed the good performance of Olivine support during the tested period of time, which was very interesting result as it is a natural and much cheaper material than alumina. Due the sorption of CO_2, it was possible to obtain hydrogen purities of 99% even with the complex mixture feeding. The sorption capacity of the sorbent strongly decreased after the first cycle, which was something that needs to be further improve.

5 Acknowledgements

The authors thank for technical and human support provided by SGIker of the University of the Basque Country (UPV/EHU). The work has been supported by a grant from Iceland, Liechtenstein and Norway through the EEA Financial Mechanism; operated by Universidad Complutense de Madrid. And also with the financial support of the Basque Government (IT993-16).

6 References

[1] M. V Gil, J. Fermoso, F. Rubiera, D. Chen, H2 production by sorption enhanced steam reforming of biomass-derived bio-oil in a fluidized bed reactor: An assessment of the effect of operation variables using response surface methodology., Catal. Today. 242 (2015) 19–34. doi:10.1016/j.cattod.2014.04.018.

[2] A. Wright, V. White, J. Hufton, E. van Selow, P. Hinderink, Reduction in the cost of pre-combustion CO2 capture through advancements in sorption-enhanced water-gas-shift, Energy Procedia. 1 (2009) 707–714. doi:https://doi.org/10.1016/j.egypro.2009.01.093.

[3] L. Zhang, R. Liu, R. Yin, Y. Mei, Upgrading of bio-oil from biomass fast pyrolysis in China: A review, Renew. Sustain. Energy Rev. 24 (2013) 66–72. doi:https://doi.org/10.1016/j.rser.2013.03.027.

[4] D. Yao, C. Wu, H. Yang, Q. Hu, M.A. Nahil, H. Chen, P.T. Williams, Hydrogen production from catalytic reforming of the aqueous fraction of pyrolysis bio-oil with modified Ni–Al catalysts, Int. J. Hydrogen Energy. 39 (2014) 14642–14652. doi:https://doi.org/10.1016/j.ijhydene.2014.07.077.

[5] A.H. Braga, E.R. Sodré, J.B.O. Santos, C.M. de Paula Marques, J.M.C. Bueno, Steam reforming of acetone over Ni- and Co-based catalysts: Effect of the composition of reactants and catalysts on reaction pathways, Appl. Catal. B Environ. 195 (2016) 16–28. doi:https://doi.org/10.1016/j.apcatb.2016.04.047.

[6] W. Nabgan, T.A. Tuan Abdullah, R. Mat, B. Nabgan, Y. Gambo, K. Moghadamian, Acetic acid-phenol steam reforming for hydrogen production: Effect of different composition of La2O3-Al2O3 support for bimetallic Ni-Co catalyst, J. Environ. Chem. Eng. 4 (2016) 2765–2773. doi:https://doi.org/10.1016/j.jece.2016.05.030.

[7] G. Esteban-Diez, M. V Gil, C. Pevida, D. Chen, F. Rubiera, Effect of operating conditions on the sorption enhanced steam reforming of blends of acetic acid and acetone as bio-oil model compounds., Appl. Energy. 177 (2016) 579–590. doi:10.1016/j.apenergy.2016.05.149.

[8] F. Zhang, N. Wang, L. Yang, M. Li, L. Huang, Ni-Co bimetallic MgO-based catalysts for hydrogen production via steam reforming of acetic acid from bio-oil., Int. J. Hydrogen Energy. 39 (2014) 18688–18694. doi:10.1016/j.ijhydene.2014.01.025.

[9] J. Chen, M. Wang, S. Wang, X. Li, Hydrogen production via steam reforming of acetic acid over biochar-supported nickel catalysts, Int. J. Hydrogen Energy. 43 (2018) 18160–18168. doi:https://doi.org/10.1016/j.ijhydene.2018.08.048.

[10] J. Fermoso, M. V Gil, F. Rubiera, D. Chen, Multifunctional Pd/Ni-Co Catalyst for Hydrogen Production by Chemical Looping Coupled With Steam Reforming of Acetic Acid., ChemSusChem. 7 (2014) 3063–3077. doi:10.1002/cssc.201402675.
[11] Y. Mei, C. Wu, R. Liu, Hydrogen production from steam reforming of bio-oil model compound and byproducts elimination, Int. J. Hydrogen Energy. 41 (2016) 9145–9152. doi:https://doi.org/10.1016/j.ijhydene.2015.12.133.
[12] I. Garcia-Garcia, E. Acha, K. Bizkarra, J. Martinez De Ilarduya, J. Requies, J.F. Cambra, Hydrogen production by steam reforming of m-cresol, a bio-oil model compound, using catalysts supported on conventional and unconventional supports, Int. J. Hydrogen Energy. 40 (2015). doi:10.1016/j.ijhydene.2015.07.155.
[13] H. Xie, Q. Yu, M. Wei, W. Duan, X. Yao, Q. Qin, Z. Zuo, Hydrogen production from steam reforming of simulated bio-oil over Ce-Ni/Co catalyst with in continuous CO2 capture., Int. J. Hydrogen Energy. 40 (2015) 1420–1428. doi:10.1016/j.ijhydene.2014.11.137.
[14] M. Marquevich, S. Czernik, E. Chornet, D. Montane, Hydrogen from Biomass: Steam Reforming of Model Compounds of Fast-Pyrolysis Oil., Energy & Fuels. 13 (1999) 1160–1166. doi:10.1021/ef990034w.
[15] A. Remiro, B. Valle, B. Aramburu, A.T. Aguayo, J. Bilbao, A.G. Gayubo, Steam Reforming of the Bio-Oil Aqueous Fraction in a Fluidized Bed Reactor with in Situ CO2 Capture., Ind. Eng. Chem. Res. 52 (2013) 17087–17098. doi:10.1021/ie4021705.
[16] G. Chen, J. Yao, J. Liu, B. Yan, R. Shan, Biomass to hydrogen-rich syngas via catalytic steam reforming of bio-oil, Renew. Energy. 91 (2016) 315–322. doi:https://doi.org/10.1016/j.renene.2016.01.073.
[17] K. Bizkarra, J.M. Bermudez, P. Arcelus-Arrillaga, V.L. Barrio, J.F. Cambra, M. Millan, Nickel based monometallic and bimetallic catalysts for synthetic and real bio-oil steam reforming, Int. J. Hydrogen Energy. 43 (2018) 11706–11718. doi:https://doi.org/10.1016/j.ijhydene.2018.03.049.
[18] D.P. Harrison, Sorption-Enhanced Hydrogen Production: A Review., Ind. Eng. Chem. Res. 47 (2008) 6486–6501. doi:10.1021/ie800298z.
[19] H. Xie, Q. Yu, W. Duan, X. Yao, X. Li, Q. Qin, Selection of CO2 sorbent used in bio-oil steam reforming process for hydrogen production, Environ. Prog. Sustain. Energy. 34 (2015) 1208–1214. doi:10.1002/ep.12083.
[20] B. Dou, C. Wang, Y. Song, H. Chen, B. Jiang, M. Yang, Y. Xu, Solid sorbents for in-situ CO2 removal during sorption-enhanced steam reforming process: A review., Renew. Sustain. Energy Rev. 53 (2016) 536–546. doi:10.1016/j.rser.2015.08.068.
[21] A. Di Giuliano, J. Girr, R. Massacesi, K. Gallucci, C. Courson, Sorption enhanced steam methane reforming by Ni–CaO materials supported on mayenite, Int. J. Hydrogen Energy. 42 (2017) 13661–13680. doi:https://doi.org/10.1016/j.ijhydene.2016.11.198.
[22] T. Noor, M. V Gil, D. Chen, Production of fuel-cell grade hydrogen by sorption enhanced water gas shift reaction using Pd/Ni-Co catalysts., Appl. Catal. B Environ. 150–151 (2014) 585–595. doi:10.1016/j.apcatb.2014.01.002.
[23] L. He, H. Berntsen, D. Chen, Approaching Sustainable H2 Production: Sorption Enhanced Steam Reforming of Ethanol., J. Phys. Chem. A. 114 (2010) 3834–3844. doi:10.1021/jp906146y.
[24] F. Bimbela, M. Oliva, J. Ruiz, L. Garcia, J. Arauzo, Hydrogen production via catalytic steam reforming of the aqueous fraction of bio-oil using nickel-based coprecipitated catalysts., Int. J. Hydrogen Energy. 38 (2013) 14476–14487. doi:10.1016/j.ijhydene.2013.09.038.
[25] U. Mann, Overview of Chemical Reaction Engineering, in: Princ. Chem. React. Anal. Des., John Wiley & Sons, Inc., 2008: pp. 1–24. doi:10.1002/9780470385821.ch1.
[26] J. Fermoso, L. He, D. Chen, Production of high purity hydrogen by sorption enhanced steam reforming of crude glycerol, Int. J. Hydrogen Energy. 37 (2012) 14047–14054. doi:10.1016/j.ijhydene.2012.07.084.
[27] A. Orio, J. Corella, I. Narvaez, Performance of Different Dolomites on Hot Raw Gas Cleaning from Biomass Gasification with Air., Ind. Eng. Chem. Res. 36 (1997) 3800–

3808. doi:10.1021/IE960810C.
[28] M. Thommes, K. Kaneko, A. V Neimark, J.P. Olivier, F. Rodriguez-Reinoso, J. Rouquerol, K.S.W. Sing, Physisorption of gases, with special reference to the evaluation of surface area and pore size distribution (IUPAC Technical Report)., Pure Appl. Chem. 87 (2015) 1051–1069. doi:10.1515/pac-2014-1117.
[29] I. Aloisi, N. Jand, S. Stendardo, P.U. Foscolo, Hydrogen by sorption enhanced methane reforming: A grain model to study the behavior of bi-functional sorbent-catalyst particles, Chem. Eng. Sci. 149 (2016) 22–34. doi:http://dx.doi.org/10.1016/j.ces.2016.03.042.
[30] Y. Hu, W. Liu, H. Chen, Z. Zhou, W. Wang, J. Sun, X. Yang, X. Li, M. Xu, Screening of inert solid supports for CaO-based sorbents for high temperature CO2 capture, Fuel. 181 (2016) 199–206. doi:https://doi.org/10.1016/j.fuel.2016.04.138.
[31] G. Taralas, Cyclohexane-steam cracking catalysed by calcined dolomite, in: D.G.B. Bridgwater, A.V.; Boocock (Ed.), Dev. Thermochem. Biomass Convers., Springer-Science, 1997: pp. 1086–1102.
[32] M. Broda, V. Manovic, Q. Imtiaz, A.M. Kierzkowska, E.J. Anthony, C.R. Müller, High-Purity Hydrogen via the Sorption-Enhanced Steam Methane Reforming Reaction over a Synthetic CaO-Based Sorbent and a Ni Catalyst, Environ. Sci. Technol. 47 (2013) 6007–6014. doi:10.1021/es305113p.
[33] D. Wierzbicki, R. Baran, R. Debek, M. Motak, T. Grzybek, M.E. Galvez, P. Da Costa, The influence of nickel content on the performance of hydrotalcite-derived catalysts in CO2 methanation reaction., Int. J. Hydrogen Energy. 42 (2017) 23548–23555. doi:10.1016/j.ijhydene.2017.02.148.